Light: Science & Applications (2013) 2, e64; doi:10.1038/lsa.2013.20

www.nature.com/lsa

ORIGINAL ARTICLE

Giant resonant light forces in microspherical photonics

Yangcheng Li[1], Oleksiy V Svitelskiy[1]*, Alexey V Maslov[2], David Carnegie[3], Edik Rafailov[3] and Vasily N Astratov[1]

Resonant light pressure effects can open new degrees of freedom in optical manipulation with microparticles, but they have been traditionally considered as relatively subtle effects. Using a simplified two-dimensional model of surface electromagnetic waves evanescently coupled to whispering gallery modes (WGMs) in transparent circular cavities, we show that under resonant conditions the peaks of the optical forces can approach theoretical limits imposed by the momentum conservation law on totally absorbing particles. Experimentally, we proved the existence of strong peaks of the optical forces by studying the optical propulsion of dielectric microspheres along tapered microfibers. We observed giant optical propelling velocities ~0.45 mm s^{-1} for some of the 15-20 μm polystyrene microspheres in water for guided powers limited at ~43 mW. Such velocities exceed previous observations by more than an order of magnitude, thereby providing evidence for the strongly enhanced resonant optical forces. We analyzed the statistical properties of the velocity distribution function measured for slightly disordered (~1% size variations) ensembles of microspheres with mean diameters varying from 3 to 20 μm. These results demonstrate a principal possibility of optical sorting of microspheres with the positions of WGM resonances overlapped at the wavelength of the laser source. They can be used as building blocks of the lossless coupled resonator optical waveguides and various integrated optoelectronics devices.
Light: Science & Applications (2013) **2,** e64; doi:10.1038/lsa.2013.20; published online 26 April 2013

Keywords: optical propulsion; optical forces; whispering gallery modes; microspheres; evanescent coupling

INTRODUCTION

Since the advent of optical[1,2] and holographic[3] tweezers the use of optical forces for trapping and propelling microparticles has become widely accepted in areas from physics to biology. In recent years, this field experienced a tremendous development due to the observation of novel mechanisms of light–matter coupling in optically bounded structures and broad application of chip-scale optical devices for particle trapping. The most notable advances include the use of diffractionless and/or engineered optical beams such as Bessel,[4,5] Airy,[6] optical lattices,[7] miniaturized fiber-optics tweezers[8] and electromagnetic fields in optically bounded structures.[9–11] These approaches stimulated observations of optical pulling forces[12] and optical lift[13] effects. Most recently, near-field optical forces have been explored in the chip-scale optical devices integrated with microfluidic systems. Designs based on nanoplasmonic structures[14–16] and photonic crystal cavities[17–19] have been developed for particle trapping.

Studies of optical propelling effects have always been of great interest for potential applications in sorting particles according to their size, index or other properties. The propelling of dielectric microspheres was studied in liquid-immersed evanescent couplers based on dielectric waveguides,[20–23] tapered fibers[24] and prisms.[25] The light pressure in such structures and devices is determined by the conservation of the total momentum along the propagation direction. It should be noted, however, that due to small reflection and absorption coefficients of dielectric spheres their propelling efficiency is greatly diminished in comparison with estimations made for totally absorbing or mirror-like particles. The propelling velocity normalized by the incident power has been found to be below ~1 mm s^{-1} W^{-1} for dielectric microspheres with diameters (D) from 2 to 20 μm.[20–25] Propelling efficiencies can be increased for strongly absorbing particles.[26] However, in the later case, the dominant mechanism of propelling has been attributed to the photophoretic forces occurring due to non-uniform heating of the light-absorbing particle.

Despite many successes and advancements in this area, one of the most important resources of optical manipulation still remains largely unexplored. It is connected with the use of internal optical resonances in microparticles for enhancing optical forces. Recently, interesting experiments on manipulating polystyrene nanoparticles in a circular motion around silica microspheres have been performed by Arnold *et al.*[27] The optical forces have been resonantly enhanced due to whispering gallery modes (WGMs) in the microspheres; however, the recipient of the optical force, the polystyrene nanoparticle, has been too small to possess resonant properties.

The subject of the present work is connected with a reverse situation when the force is enhanced by the resonance in the moving microsphere. Due to inevitable ~1% microsphere diameter variations and the size-dependent nature of WGMs resonances, this effect can be used for sorting microspheres with WGM peaks overlapped at the

[1]Department of Physics and Optical Science, Center for Optoelectronics and Optical Communication, University of North Carolina at Charlotte, Charlotte, NC 28223-0001, USA; [2]Department of Radiophysics, University of Nizhny Novgorod, Nizhny Novgorod 603950, Russia and [3]Photonics and Nanoscience Group, School of Electrical Engineering and Physics, University of Dundee, Nethergate, Dundee DD1 4HN, UK
*Current address: Colgate University, Hamilton, NY 13346, USA
Correspondence: Professor VN Astratov, Department of Physics and Optical Science, University of North Carolina at Charlotte, Charlotte, North Carolina 28223-0001, USA
E-mail: astratov@uncc.edu
Received 30 August 2012; revised 25 November 2012; accepted 17 December 2012

wavelength of the laser source. This is a highly attractive property for fundamental studies and applications of coupled cavity structures and devices.[28–33] It should be noted, however, that although the resonant forces have been observed in microdroplets by the pioneer of optical tweezers himself, Arthur Ashkin, more than 30 years ago,[34] these effects were relatively weakly pronounced. Some evidence for the resonance force enhancement has been obtained in waveguide couplers[35] and in the case of off-axially shifted focused beams.[36] More recently, the notable advance in this field has been made based on theoretical demonstration of high peak-to-background resonant force ratios in evanescent prism couplers.[37,38] However, many properties of resonant light forces still await a thorough investigation.

In the present work, we first present results of our calculation of the optical forces exerted on circular cavities in a simplified two-dimensional (2D) model of surface electromagnetic waves. We show that the resonant forces can approach and even exceed the limits established for totally absorbing particles. After that, we present our experimental observations of propelling of polystyrene microspheres in the near-field vicinity of tapered microfibers immersed in water. For a certain small fraction of spheres with $D \approx 15$–20 μm, we observed giant power normalized propelling velocities ~10 mm s^{-1} W^{-1} that exceed the previous measurements in various evanescent couplers[20–25] by more than an order of magnitude. These extraordinary high propelling efficiencies approach estimations made in a total absorption limit that indicates that a significant part of the total guided power is used for the creating light pressure. We also performed analysis of statistical distribution of the propelling velocities for a large number of microspheres with ~1% size variations and with mean diameters from 3 to 20 μm. We explain these results using a concept of resonant enhancement of the optical force due to WGM coupling effects. These effects can be used for sorting microspheres with WGM peaks overlapping in the vicinity of the laser source wavelength λ_0: $\Delta\lambda/\lambda_0 < 1/Q$, where $\Delta\lambda$ is the WGM peak detuning and Q is the WGM's quality factor. Taking into account that $Q \approx 10^3$–10^4 are common for liquid-immersed microspheres,[39] it opens up a unique way of selecting the building blocks of chip-scale structures with resonantly coupled WGMs for applications in coupled resonator optical waveguides and coupled cavity devices.

THEORETICAL MODELING OF RESONANT FORCES

To study the optical forces that can act on WGM resonators we begin with the physical model illustrated in Figure 1a. An initial surface wave with frequency ω is guided by the boundary of the lower half-space with dielectric constant $\varepsilon_m < 0$. The upper half-space has refractive index n_b. A dielectric cylinder with refractive index n_s is located at a distance d from the boundary. When the surface wave interacts with the cylinder, it can excite the WGMs of the cylinder. The material

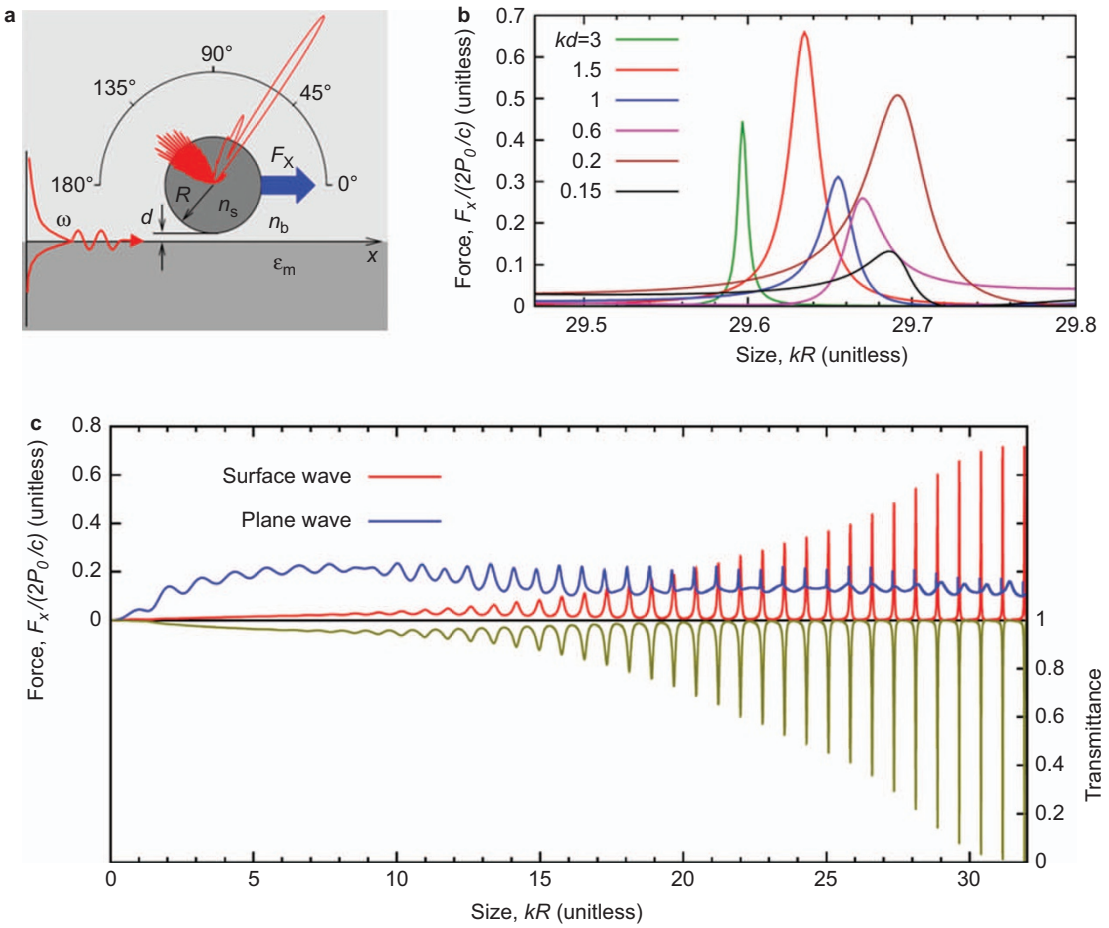

Figure 1 (**a**) Schematic of the illumination of a cylinder by a surface wave with the frequency ω guided by the boundary of a half-space with $\varepsilon_m < 0$. The scattering of the surface wave (the typical far field directionality of bulk radiation at resonance is shown in red) creates the propelling force F_x along the surface. (**b**) Size dependence of the resonant force on the cylinder for various values of the cylinder-boundary separation. (**c**, top frame) Size dependence of the propelling force on the size parameter kR for the excitation by a surface wave (red curve corresponds to $kd = 1.5$) and by a plane wave (blue curve). (**c**, bottom frame). Transmittance for the surface wave (olive curve corresponds to $kd = 1.5$).

doi:10.1038/lsa.2013.20

parameters used in the simulations are $\varepsilon_m=-2$, $n_b=1$, $n_s=1.4$. Since the material parameters are frequency independent the solution depends only on two dimensionless size parameters kR and kd, where $k=\omega/c$ is the wavenumber and c is the speed of light in vacuum. This 2D model captures the basic phenomena important for this study such as the excitation of the WGM by an evanescent tail, the interaction of the excited mode with the guiding structure, and the creation of the scattered field.

The scattering of a guided wave by a resonator is a complicated diffraction problem. Often this problem is solved by expanding the initial guided wave in terms of the modes of the resonator in free space.[40] However, such an expansion is only an approximation and an accurate solution would require the use of the modes of the combined system, e.g., the waveguiding structure and resonator. This approximation is expected to become less accurate as the distance between the resonator and the surface decreases. In our experiments, the separation varied greatly and even reached the values significantly smaller than the wavelength. We therefore resorted to a more rigorous approach that would allow us to obtain accurate results in a wide range of distances.

Our solution is based on the surface potential method[41–43] applied to the model shown in Figure 1a. We reduce the Maxwell equations to the wave equation for the magnetic field which has only one component oriented along the cylinder axis. Then we express the scattered field outside of the cylinder in terms of the single layer surface potential on the surface of the cylinder and Green's function for the two half-spaces. The surface potential is expanded in terms of the angular exponential functions. The total field inside the cylinder is expanded in terms of the cylindrical functions. We match the expansions inside and outside the cylinder by using the continuity condition for the magnetic field component and for the tangential electric field component. This matching gives an infinite system of linear algebraic equations for the expansion coefficients. By truncating the system and solving it numerically, we find the coefficients and therefore, the electromagnetic fields inside and outside of the cylinder. In particular, we find the amplitudes of the transmitted and reflected surface waves, as well as the distribution of the far field radiation. The electromagnetic force follows directly from the fields.

We verified the correctness of the numerically calculated fields by checking the balance between the power of the initial surface wave and the sum of powers of the transmitted and reflected waves and the bulk radiation in the far field region. The calculation of force was verified by obtaining an agreement between two approaches: by integrating the Lorentz force (with electric and magnetic components) over the cylinder cross section and by integrating the Maxwell tensor outside of the cylinder.

A plane wave propagating in vacuum and reflected from a mirror creates a force $2P_0/c$, where P_0 is the power incident on a given area.[44] In the case of a partial reflection, the force on the mirror will be smaller and, for example, becomes P_0/c for a compete absorption. For surface waves, it is therefore instructive to investigate the ratio of the force and the quantity $2P_0/c$, where P_0 is the power of the surface wave, as an indicator of the efficiency of using the surface waves to propel WGM micro-resonators.

A comparison of the force created by a surface wave of power P_0 and a plane wave that has power P_0 per area of size $2R$ in the transverse direction is presented in Figure 1c. In both cases, the presence of resonant forces for sizes $kR>10$ is apparent. For the plane wave, the peak amplitudes and peak-to-background ratios are limited while for the surface wave both the peak amplitudes and peak-to-background ratios increase monotonically with kR reaching extremely high values. The strongly peaked forces correlate well with the dips in the transmittance spectrum for the surface wave. When the transmittance almost vanishes for large values of $kR\approx30$, the normalized force can reach a value around 0.7. This means that the surface wave can propel the transparent cylinder by means of WGM excitation more efficiently than a plane wave can propel a totally absorbing cylinder. For a plane wave in vacuum, such a large value of force would correspond to a significant reflection. For WGM mode, the reflected surface wave is practically negligible and the incident power is distributed between the transmitted surface wave and bulk radiation. A typical example of the far field directionality of bulk radiation is illustrated in Figure 1a. It demonstrates the lobe at ~57° with the direction of the initial wave propagation, but there is indeed a significant scattering in a range of backward directions at ~120°–150°. The larger value of force as compared to that for a plane wave can also be attributed to a larger momentum carried by the surface wave.[45]

The behavior of the resonant propelling force near a selected resonance for various values of distances from the surface is illustrated in Figure 1b. Starting from a large $kd>>3$ (not shown in Figure 1b), the peak force increases with decreasing kd. The maximum force is obtained at $kd\approx1.5$. The non-monotonic behavior of the magnitude of the optical force at $kd<1.5$ can be related to interference effects; however, this requires a more detailed analysis. An important consequence for possible optical propelling experiments consists in a substantial overlap of the calculated force peaks for a range of separations $0.15<kd<0.6$. A similar peak overlap should take place in the spectral domain for a sphere with $kR=29.68-29.69$. Once the laser source is tuned into this resonance, the moving particle would experience an enhanced propelling force for a range of separations from the boundary that should simplify the experimental observation of this effect. In principle, similar physical effects take place in various evanescent couplers including dielectric waveguides or tapered fibers.

MATERIALS AND METHODS

Microfluidic fiber-integrated platform

Observation of resonant propelling effects requires the presence of a strong evanescent field in a liquid environment containing microspheres. Tapered microfibers provide a number of advantages compared to other evanescent couplers in such experiments.[39] These include small optical losses on the level of a few decibels, natural integration with fiber-optics based light sources and spectrometers, and the possibility to control the flow of the microspheres, as schematically illustrated in Figure 2a. We obtained adiabatically tapered fibers by etching of a single mode fiber SMF-28 in a droplet of hydrofluoric acid.[46] This technique allows obtaining tapers with ~1.5 μm diameters and millimeter-scale lengths. The tapered fibers were integrated with a microfluidic platform fabricated using a Plexiglas frame depicted in Figure 2a. The frame was fixed at the top of the microscope slide to create a microfluidic cell with unrestricted optical access. We selected polystyrene microspheres (Duke Standards* 4000 Series Monosized Particles; Thermo Fisher Scientific, Fremont, CA, USA) for propelling experiments because of their ability to float in water due to the fact that the specific gravity of polystyrene in water is ~1.05.

Fiber-taper-coupled microsphere system

Observation of resonant propelling effects also requires efficient WGM coupling determined by the depth of the dip in the power transmission spectra which can be approximated in a single-mode

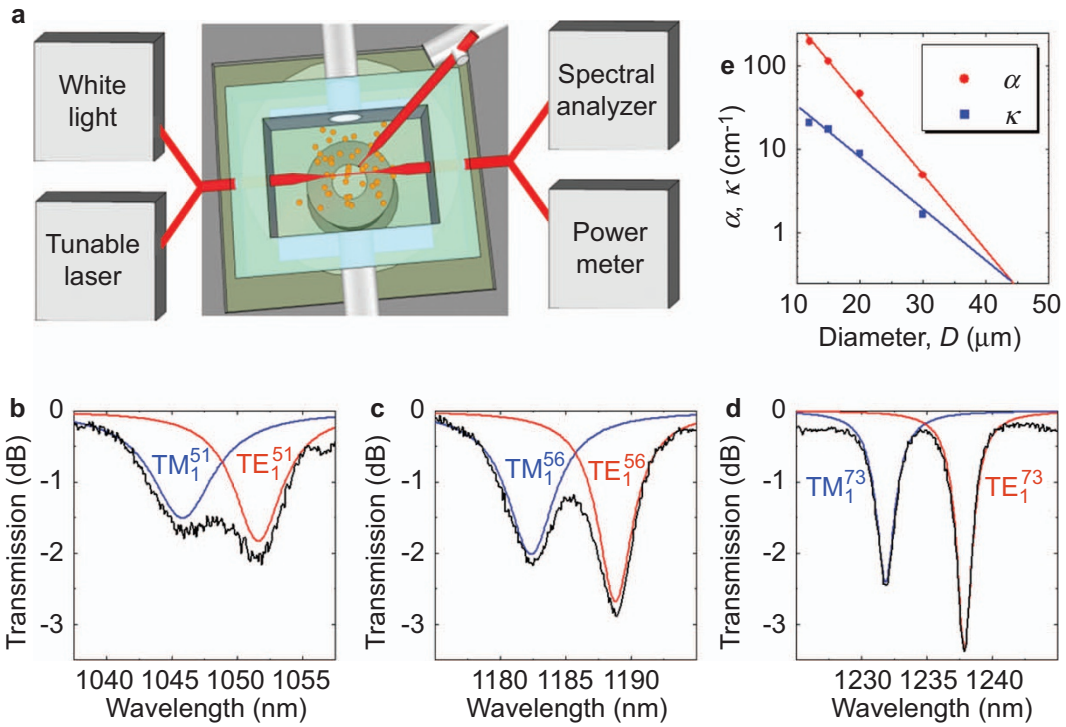

Figure 2 (**a**) Microfluidic fiber-integrated platform. (**b–d**) Transmission of 1.5 μm diameter fiber in contact with single water-immersed polystyrene spheres with D=12, 15 and 20 μm, respectively. The WGM polarizations and numbers are labeled. Red and blue curves represent results of fitting with Equation (1). (**e**) Size dependence of the phenomenological coupling parameters α and κ illustrating weak coupling regime with a critical coupling expected at D≈44 μm.

model:[47]

$$P = e^{-\gamma} \times \frac{(\beta-\beta_0)^2+(\gamma/2S+\alpha-\kappa)}{(\beta-\beta_0)^2+(\gamma/2S+\alpha+\kappa)} \qquad (1)$$

Here, κ is the coupling constant, $\beta=2\pi n_s/\lambda$ is the propagation constant ($\beta_0=2\pi n_s/\lambda_0$), n_s is the sphere index, α is the field attenuation coefficient inside the sphere, γ is the coupling loss and $S=\pi D$ is the circumference of the circle in the equatorial plane. In a weak coupling regime ($\kappa<\alpha$) which usually takes place for various compact (D<20 μm) water-immersed spheres,[39] the depth of the resonant dip in transmission spectra increases with the coupling constant κ.

To identify the range of sphere diameters most suited for observation of resonant propelling effects we determined how both parameters, κ and α, depend on D. This was studied by bringing polystyrene (n_s=1.59) spheres in a contact position with the same section of silica taper. Microspheres were individually micromanipulated using a sharpened fiber as a stick. The transmission spectra were measured using a white light source (AQ4305; Yokogawa Corp. of America, Newnan, GA, USA) and optical spectral analyzer (AQ6370C-10; Yokogawa Corp. of America), as shown in Figure 2a.

Figure 2b–d displays a typical evolution of WGM-based coupling features observed in fiber transmission spectra for D=12, 15 and 20 μm, respectively. The spatial WGM properties in microspheres are described by three modal numbers, radial n, angular l and azimuthal m.[28,33] The radial number, n, represents the number of the intensity maxima along the radial direction. The angular number, l, shows the number of modal wavelengths around the circumference of the sphere at the equator which can be estimated as $\pi D \approx l(\lambda/n_s)$. The azimuthal number, m, describes the number of the intensity maxima in a direction perpendicular to the equator according to the formula $l-m+1$ with the case $m=l$ representing a fundamental mode in the equatorial plane. The azimuthal modes are degenerate in a perfect free-standing sphere. This degeneracy can be lifted by small uncontrollable ellipticity (~1%) of the real physical beads. The partial overlap of the modes with different m numbers can be responsible for the broadening of the WGM spectral features. It is likely that the dips observed in Figure 2b–d are inhomogeneously broadened due to this effect. Determination of m numbers is not possible in this situation, however n and l numbers as well as the WGMs polarizations, TE_n^l or TM_n^l, can be identified for different dips, as shown in Figure 2b–d. The mode assignment requires fitting the positions of the resonances in a broad spectral range using the Mie scattering theory.[39,48]

As illustrated in Figure 2e, the fiber-taper-coupled microsphere system operates in a weak coupling regime for spheres with D in 12–30 μm range. Although the maximal resonant optical forces are expected at critical coupling ($\kappa=\alpha$) around D≈44 μm, these spheres are too bulky and their narrow first order (n=1) resonances with $Q\approx10^5$ are difficult to use in practical optical propelling experiments. On the other hand, spheres with $15 \leqslant D \leqslant 20$ μm and $Q\approx10^3$ provide much better trade-off between their compact dimensions and efficiency of WGM-based coupling. For the 20 μm spheres, the depth of the resonant dips was found to be about 3.5 dB, which means that more than a half of the optical power (~55%) was transferred into the spherical cavity. Assuming approximately uniform directionality of light scattering, the peak of the resonant force can approach the absorption limit ($\sim 0.55\times P_0/c$) in this case.

RESULTS AND DISCUSSION

The conventional approach to studying propelling effects is based on using a laser source and an imaging system to visualize light-induced motions of individual particles. The spheres which happen to be in a

doi:10.1038/lsa.2013.20

micrometer-scale vicinity of the evanescent field are attracted to the core by the optical gradient force. After that they can be propelled along the fiber due to the scattering optical forces, as illstrated in the inserts of Figure 3. The particles reach a terminal velocity (v) when the scattering force (F_x) is equal to the drag force, $C=6\pi\mu Rv$, where μ is the dynamic viscosity.[20–25]

Due to the focus of the present study on resonant light pressure effects, we modified the conventional experimental approach to propelling measurements by evanescent fields[20–25] in regard to the following factors: (i) range of sphere diameters was increased up to $3\leqslant D\leqslant 20$ μm (compared to previously studied $D<10$ μm range); (ii) instead of the average propelling velocities ($v_{av}=<v>$), we measured maximal instantaneous propelling velocities ($v_{max}=\max(v)$); and (iii) statistical distribution of v_{max} was studied as a function of D.

Variation of the sphere diameters in a microfluidic platform

Propelling of spheres with different diameters was realized by using a number of suspensions with various mean D values and ~1% diameter variations in each suspension. A slow flux (~10 μm s^{-1}) of suspension of microspheres was produced perpendicular to the taper by a micropump (M100; TCS Micropumps Ltd, Ospringe, UK) included in a closed microfluidic loop. Since the parameters of individual tapers such as the thickness of the tapered region were difficult to precisely control, all propelling events were recorded for the same section (~300 μm length) of the same tapered fiber. After completing measurements for a given sphere diameter the microfluidic platform was cleaned and infiltrated with a suspension containing spheres with different D.

The optical power was coupled from a single mode tunable (1160–1280 nm) semiconductor laser (TOPTICA Photonics AG, Gräfelfing, Germany).[49] Due to small scattering losses (~3 dB) in the tapered region we were able to control the total guided power (P_0) at the waist of the taper with ~5% precision. The propelling velocity is expected to be almost linearly dependent on P_0 for spheres with $D<10$ μm.[20–25] In order to study the dependence of propelling as a function of D, we fixed the power at the taper waist for all measurements at relatively modest level of $P_0=43\pm2$ mW. The laser emission linewidth was narrower than 0.1 nm and is smaller than the width of any WGM resonances studied in this work. It was fixed around $\lambda_0=1200$ nm, and the results did not strongly depend on the selection of λ_0. In our experiments variation of the detuning, $\Delta\lambda=\lambda-\lambda_0$, between the laser emission and WGM resonances (λ) was realized due to random ~1% deviations of the sphere diameters.

It should be noted that the spheres tend to be separated from the fiber by a nanometric gap occurring due to the double layer repulsive forces between the similarly charged particle and fiber.[22] The origin of this gap has been studied in experiments on a WGM carousel, a photonic mechanism for trapping polystyrene nanoparticles in a circular motion around silica microspheres.[27] It has been demonstrated that the particle is radially trapped due to a combination of a long-range attractive interaction and a short-range repulsive interaction. The attractive optical force originates from the radial gradient of the evanescent fields. The repulsive electrostatic force is connected with similarly (negatively) charged bare surface of the silica fiber and polystyrene nanoparticles. The average gap sizes have been estimated to be around 35 nm.[27] In our work, we used significantly larger polystyrene microspheres. It is likely that in the course of propulsion the radial gap sizes can vary in a certain range that can lead to a variation of the optical force. In addition, the average size of this gap should depend on P_0, D, and on the concentration of ions in a suspension. It is likely that the average size of these gaps in our experiments was on the scale of few tenths of nanometers;[22,27] however, additional studies are required for more precise characterization of the gap sizes. This plays a critical role in achieving steady propelling along the fiber, because the spheres were covered with a sticky surfactant layer by the manufacturer and physical contact with the fiber would retard their motion. It should also be noted that the small nanoscale gap sizes expected in our case mean that we can use fiber transmission spectra obtained in contact with sphere (Figure 2) for qualitative understanding of the possible role of WGM coupling effects in the course of propelling.

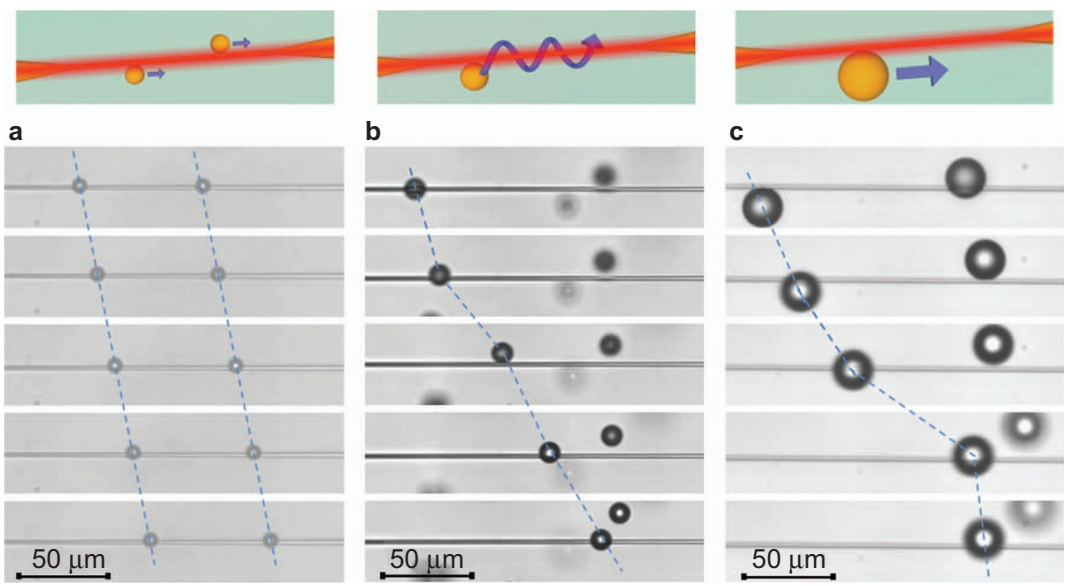

Figure 3 Sequences of snapshots taken with 160 ms time intervals illustrating propelling of polystyrene spheres with different D: (**a**) 7 μm, (**b**) 10 μm and (**c**) 20 μm spheres. Laser light propagates from left to right. Inserts at the top of (**a–c**) schematically illustrate the type of sphere motion represented by the corresponding consecutive photos. Propelling of 7 μm spheres in (**a**) is very steady with $v_{max}\approx v_{av}$. Propelling of 10 μm sphere in (**b**) shows some variations of the particle velocity. Propelling of 20 μm spheres in (**c**) demonstrates giant instantaneous velocity between the third and fourth snapshots (counted from top down) reaching $v_{max}\approx0.45$ mm s^{-1}.

Velocity measurement

The radiative pressure effects were studied by recording movies[50] of individual propelling events for each D in inverted microscope (IX71; Olympus America Inc., Center Valley, PA, USA) using CCD camera (Olympus MicroFire; Olympus America Inc., Melville, NY, USA). The frames were sufficiently short (~5 ms) to represent the snapshots of the spheres' motion. They were separated by ~160 ms time intervals.

Typical propelling effects for spheres with D=7, 10 and 20 μm are represented by consecutive photos in Figure 3a–c, respectively. The sequence of snapshots taken for the 7 μm spheres shows motion with constant velocity, as illustrated by dashed construction lines in Figure 3a (a video of the propelling 7 μm spheres is provided in Supplementary Movie 1). We found that propelling with constant velocity was typical for each sphere size in the range $3 \leqslant D \leqslant 7$ μm; however, the velocity is higher for larger spheres. After propelling over a distance on the order of 100 μm (or longer in some cases), the spheres eventually depart the fiber. This can happen due to fluctuations in the liquid flux or due to moving to a wider section of the taper where the evanescent fields are weaker. The motion of 10 μm spheres is less steady demonstrating deviations of the 'instantaneous' velocity measured between neighboring frames from the velocity averaged over several frames, as seen in Figure 3b. The particles can also spiral along the taper in some cases, as can be also seen in Figure 3b.

For $15 \leqslant D \leqslant 20$ μm spheres, the variations in instantaneous velocity becomes a dominant factor, as illustrated for D=20 μm in Figure 3c (a video of the propelling 20 μm spheres is provided in Supplementary Movie 2). The likely explanation for this effect is connected with the fact that larger (and more massive) particles have an increased probability of touching the fiber causing the sphere to brake. There might also be other reasons for the seemingly discontinuous motion of the larger spheres based on rapidly varying resonant effects. It is likely that the spheres are rotating along their own axis in the course of the propelling. This can lead to coupling with azimuthal modes with varying m numbers which can be split in energy due to uncontrollable ellipticity (~1%) of the real physical beads. The variations of the gap sizes can be another reason for discontinuous motion of the larger spheres.

Since we are interested in unrestricted motion of spheres in situations where the light-pressure effects are maximally pronounced, we analyzed long propelling movies to find the maximal velocity measured between neighboring frames, v_{max}, for each propelling event. In the example shown in Figure 3c such maximal velocity is evident due to ~70 μm jump of 20 μm sphere between third and fourth frame leading to extraordinary high value of $v_{max} \approx 0.45$ mm s^{-1}. Such v_{max} reaches ~60% of the terminal velocity estimated in the total absorption limit: $v = P_0/(3\pi c\mu D) \approx 0.76$ mm s^{-1}. In units normalized by the optical power the measured velocity corresponds to ~10 mm s^{-1} W^{-1} which exceed previously published data for different evanescent couplers[20–25] by more than an order of magnitude. Taking into account that conventional optical forces on transparent microspheres cannot exceed a few percent of the force estimated in the total absorption limit, the only plausible explanation for the observed extraordinarily high velocities is based on the mechanism of resonantly enhanced optical force.

Statistical properties of propelling

The dramatic difference in propelling of small, $3 \leqslant D \leqslant 7$ μm, and large, $15 \leqslant D \leqslant 20$ μm, particles is illustrated in a greater detail by v_{max} measurements for a broad range of mean sphere diameters represented in Figure 4a. For each mean sphere diameter the measurements

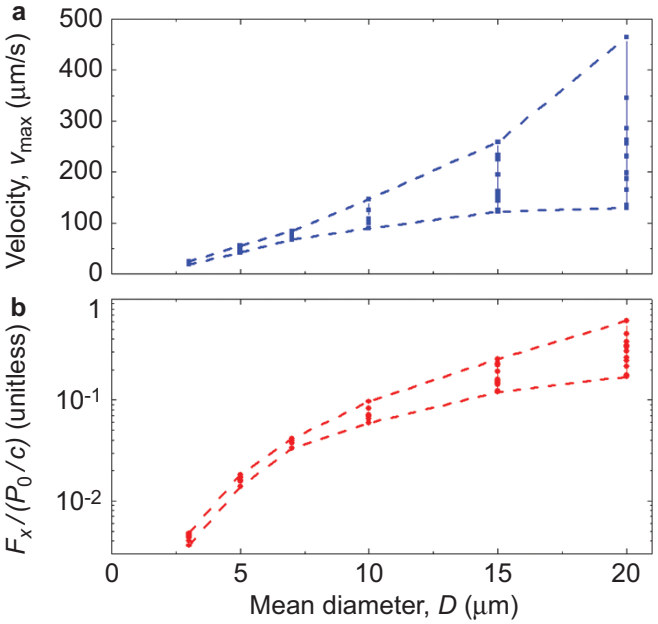

Figure 4 Results of multiple measurements of (**a**) maximal instantaneous propelling velocity (v_{max}) and (**b**) normalized propelling force ($F_x/(P_0/c)$, where $F_x = 3\pi\mu D v_{max}$) for polystyrene spheres with different mean diameters, D=3, 5, 7, 10, 15 and 20 μm. For each mean diameter up to 20–40 measurements were performed using spheres with random ~1% diameter variations.

were repeated for many spheres with ~1% diameter variations. The purpose of these studies was to see how this size disorder would translate into the distribution of propelling velocities. It is seen that for small spheres the velocity is well reproducible for each mean diameter (D=3, 5 and 7 μm) irrespective of the ~1% size variations. In this range of sphere sizes, we found almost linear dependence of v_{max} on the sphere diameter in agreement with the previous studies performed in waveguide couplers.[20–25] The linear dependence can be understood due to the fact that the nonresonant scattering force is proportional to the interaction volume, whereas the drag force is proportional to the sphere cross-section.

For large spheres with $15 \leqslant D \leqslant 20$ μm multiple measurements revealed extremely broad v_{max} distribution in striking contrast with the case of small spheres. Such behavior is expected for resonantly enhanced forces. As illustrated in Figure 2c and d, the WGM resonances with $Q \approx 10^3$ are well pronounced for such spheres. If the laser wavelength matches the position of the WGM resonance, the propelling force should be resonantly enhanced due to a mechanism illustrated for a simplified 2D model in Figure 1b and c. On the other hand, the nonresonant propelling forces (laser line is between the WGM peaks) tend to vanish for sufficiently large circular cavities. Random ~1% diameter variations should lead to a broad (~10 nm) distribution of detuning between the laser and WGMs in different spheres. Only a small fraction of spheres with WGM peak position overlapped with the laser line are expected to be propelled along the fiber. For these spheres, the optical forces are expected to display dramatic variations from sphere to sphere depending of the precise amount of small detuning (below ~1 nm) between the laser and WGMs peak positions. This should lead to a broad distribution of velocities v_{max} and scattering forces F_x for large spheres, consistent with the results presented in Figure 4a and b, respectively.

To study the transition from nonresonant to resonant propelling effects in a greater detail, we analyzed probability distribution histograms

doi:10.1038/lsa.2013.20

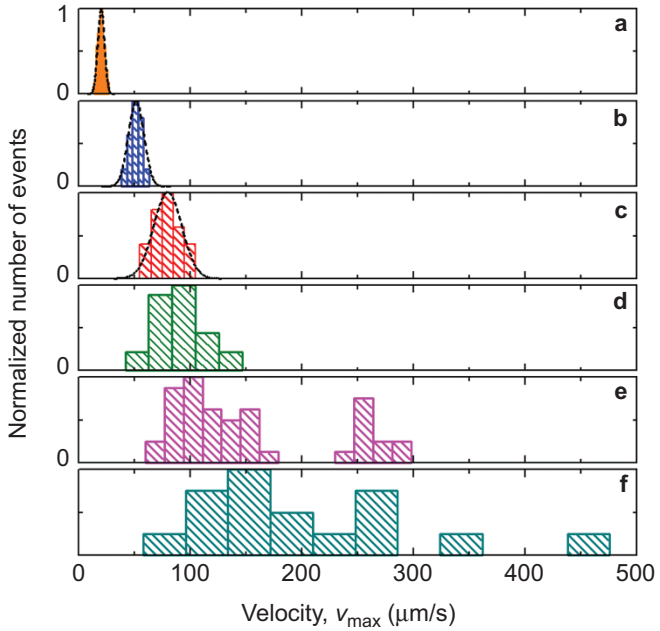

Figure 5 Probability distribution histograms for v_{max} values measured for spheres with different mean diameters *D*: (**a**) –3 μm, (**b**) –5 μm, (**c**) –7 μm, (**d**) –10 μm, (**e**) –15 μm, (**f**) –20 μm. For each mean diameter up to 20–40 measurements were performed using spheres with random ~1% diameter variations. The fitting curves in **a**–**c** are represented by normalized Gaussian probability density distributions, $f \approx \exp[(v_{max}-v_{max0})^2/2\sigma^2]$, where v_{max0} is the average v_{max} and σ is the standard deviation. It is seen that for small $3 \leqslant D \leqslant 7$ μm spheres the distributions have Gaussian shape with narrow width $\sigma/v_{max0} \approx 15\%$. For large $15 \leqslant D \leqslant 20$ μm spheres the distributions are extremely wide. The case of 10 μm spheres can be considered as a transitional between these two situations.

for v_{max} values measured for multiple spheres with ~1% size variations, as illustrated in Figure 5. The maximum of the distribution histogram was normalized. For small spheres with $3 \leqslant D \leqslant 7$ μm the histograms represent relatively narrow Gaussian-like distributions with ~15% standard deviation, as shown in Figure 5a–c. For 10 μm spheres, the distribution becomes much broader which can be interpreted as being due to the onset of resonant propelling effects. For 15 and 20 μm spheres, the distributions become extremely wide demonstrating velocities varying for different spheres by a factor of 4 and 6 in Figure 5e and f, respectively. It should be noted that, due to limited experimental statistics and a somewhat arbitrary determination of the maximal propelling velocity from the experimental movies, the shape of these distributions is not precisely defined in Figure 5e and f. It is apparent, however, that the width and shape of these distributions is strikingly different from the narrow Gaussian-like distributions observed for small spheres, indicating that they are determined by the resonant optical forces.

Such a significant increase of v_{max} in resonant cases can be used for developing devices capable of sorting microspheres with WGM peaks overlapped with the laser wavelength λ_0, $\Delta\lambda/\lambda_0 < 1/Q$. Taking into account ~1% diameter variations in the initial suspensions, the resonant WGMs in thus selected spheres might have different angular *l* numbers; however, such WGMs can still be efficiently coupled[51] in structures and devices formed by multiple spheres in a contact position.

CONCLUSIONS

We experimentally observed giant optical propelling velocities of 15–20 μm polystyrene microspheres in evanescent fiber-to-microsphere couplers. The normalized propelling velocities measured in our work ~10 mm s^{-1} W^{-1} exceed previous observations[20–25] by more than an order of magnitude. The magnitude of the corresponding forces reaches 60% of maximal possible force in the total absorption limit. We interpret these observations by resonant enhancement of the optical force due to evanescent coupling to WGMs in microspheres. This interpretation is consistent with our numerical estimations of the peak forces in a simplified 2D model of surface electromagnetic waves evanescently coupled to circular cavities. It is also supported by the statistical analyses of the propelling velocity measurements performed for multiple spheres with ~1% size variations and with different mean diameters.

These effects can be used for sorting cavities with WGMs peaks which are resonant with the wavelength of the laser source within ~1/*Q* relative accuracy. By using a tunable laser the spheres with the desired positions of WGM peaks can be selected. Depending on the application, the method of sorting cavites by using resonant light pressure can be a much more accurate and flexible technique compared to standard in-plane fabrication of coupled microrings and microdisks.[52] Microspheres with resonant WGMs can be used as building blocks of delay lines,[30] ultra-narrow spectral filters, laser-resonator arrays,[53] waveguides,[29–32] focusing devices,[54,55] microspectrometers[56] and sensors.[57] Such spheres are also required in biomedical applications[58] where they are used as markers, fluorescent labels and spectral fingerprints.

ACKNOWLEDGMENTS

The authors thank Ilya Vitebskiy, Vassilios Kovanis and Nicholaos Limberopoulos for stimulating discussions. YL, OVS and VNA gratefully acknowledge support for our work from the US Army Research Office (ARO) under grant W911NF-09-1-0450 and DURIP W911NF-11-1-0406 and W911NF-12-1-0538 (John T Prater), and from the National Science Foundation (NSF) under grant ECCS-0824067. AVM gratefully acknowledges a partial support from the Ministry of Education and Science of the Russian Federation through agreement no. 14.B37.21.0892. DC and ER gratefully acknowledge a partial support from the EU FP7 program through FAST-DOT project (contract no. 224338). We are also thankful to Thermo Fisher Scientific, Inc. for donating microspheres for this work.

1 Ashkin A. Acceleration and trapping of particles by radiation pressure. *Phys Rev Lett* 1970; **24**: 156–159.
2 Ashkin A, Dziedzic JM, Bjorkholm JE, Chu S. Observation of a single-beam gradient force optical trap for dielectric particles. *Opt Lett* 1986; **11**: 288–290.
3 Grier DG. A revolution in optical manipulation. *Nature* 2003; **424**: 810–816.
4 Arlt J, Garcés-Chávez V, Sibbett W, Dholakia K. Optical micromanipulation using a Bessel light beam. *Opt Commun* 2001; **197**: 239–245.
5 McGloin D, Dholakia K. Bessel beams: diffraction in a new light. *Contemp Phys* 2005; **46**: 15–28.
6 Baumgartl J, Mazilu M, Dholakia K. Optically mediated particle clearing using Airy wavepackets, *Nat Photon* 2008; **2**: 675–678.
7 MacDonald MP, Spalding GC, Dholakia K. Microfluidic sorting in an optical lattice. *Nature* 2003; **426**: 421–424.
8 Liberale C, Minzioni P, Bragheri F, de Angelis F, Di Fabrizio E *et al*. Miniaturized all-fibre probe for three-dimensional optical trapping and manipulation. *Nat Photon* 2007; **1**: 723–727.
9 Mellor CD, Bain CD. Array formation in evanescent waves. *Chem Phys Chem* 2006; **7**: 329–332.
10 Karasek V, Cizmar T, Brzobohaty O, Zemanek P, Garcés-Chávez V *et al*. Long-range one-dimensional longitudinal optical binding. *Phys Rev Lett* 2008; **101**: 143601.
11 Dholakia K, Zemanek P. Colloquium: crippled by light: optical binding. *Rev Mod Phys* 2010; **82**: 1767–1791.
12 Chen J, Ng J, Lin Z, Chan CT. Optical pulling force. *Nat Photon* 2011; **5**: 531–534.
13 Swartzlander GA, Peterson T, Artusio-Glimpse AB, Raisanen AD. Stable optical lift. *Nat Photon* 2011; **5**: 48–51.
14 Righini M, Zelenina AS, Girard C, Quidant R. Parallel and selective trapping in a patterned plasmonic landscape. *Nat Phys* 2007; **3**: 477–480.
15 Grigorenko AN, Roberts NW, Dickinson MR, Zhang Y. Nanometric optical tweezers based on nanostructured substrates. *Nat Photon* 2008; **2**: 675–678.

16 Juan ML, Righini M, Quidant, R. Plasmon nano-optical tweezers. *Nat Photon* 2011; **5**: 349–356.
17 Barth M, Benson O. Manipulation of dielectric particles using photonic crystal cavities. *Appl Phys Lett* 2006; **89**: 253114.
18 Lin S, Hu J, Kimerling L, Crozier K. Design of nanoslotted photonic crystal waveguide cavities for single nanoparticle trapping and detection. *Opt Lett* 2009; **34**: 3451–3453.
19 Ma J, Martínez LJ, Povinelli ML. Optical trapping via guided resonance modes in a Slot-Suzuki-phase photonic crystal lattice. *Opt Express* 2012; **20**: 6816–6824.
20 Grujic K, Helles OG, Wilkinson JS, Hole JP. Optical propulsion of microspheres along a channel waveguide produced by Cs^+ ion-exchange in glass. *Opt Commun* 2002; **239**: 227–235.
21 Gaugiran S, Gétin S, Fedeli JM, Colas G, Fuchs A *et al*. Optical manipulation of microparticles and cells on silicon nitride waveguides. *Opt Express* 2005; **18**: 6956–6963.
22 Schmidt BS, Yang AHJ, Erickson D, Lipson M. Optofluidic trapping and transport on solid core waveguides within a microfluidic device. *Opt Express* 2007; **22**: 14322–14334.
23 Yang AHJ, Moore SD, Schmidt BS, Klug M, Lipson M *et al*. Optical manipulation of nanoparticles and biomolecules in sub-wavelength slot waveguides. *Nature* 2009; **457**: 71–75.
24 Brambilla G, Murugan GS, Wilkinson JS, Richardson DJ. Optical manipulation of microspheres along a subwavelength optical wire. *Opt Lett* 2007; **32**: 3041–3043.
25 Marchington RF, Mazilu M, Kuriakose S, Garcés-Chávez V, Reece PJ *et al*. Optical deflection and sorting of microparticles in a near-field optical geometry. *Opt Express* 2008; **16**: 3712–3726.
26 Shvedov VG, Rode AV, Izdebskaya YV, Desyatnikov AS, Krolikowski W *et al*. Giant optical manipulation. *Phys Rev Lett* 2010. **105**: 118103.
27 Arnold S, Keng D, Shopova SI, Holler S, Zurawsky W *et al*. Whispering gallery mode carousel—a photonic mechanism for enhanced nanoparticle detection in biosensing. *Opt Express* 2009; **17**: 6230–6238.
28 Astratov VN. Fundamentals and Applications of Microsphere Resonator Circuits. In: Chremmos I, Schwelb O, Uzunoglu N, editors. Photonic Microresonator Research and Applications. Vol. 156, Chapter 17. New York: Springer Series in Optical Sciences; 2010. pp423–457. http://link.springer.com/chapter/10.1007%2F978-1-4419-1744-7_17.
29 Astratov VN, Franchak JP, Ashili SP. Optical coupling and transport phenomena in chains of spherical dielectric microresonators with size disorder. *Appl Phys Lett* 2004; **85**: 5508–5510.
30 Hara Y, Mukaiyama T, Takeda K, Kuwata-Gonokami M. Heavy photon states in photonic chains of resonantly coupled cavities with supermonodispersive microspheres. *Phys Rev Lett* 2005; **94**: 203905.
31 Kapitonov AM, Astratov VN. Observation of nanojet-induced modes with small propagation losses in chains of coupled spherical cavities. *Opt Lett* 2007; **32**: 409–411.
32 Yang S, Astratov VN. Photonic nanojet-induced modes in chains of size-disordered microspheres with an attenuation of only 0.08 dB per sphere. *Appl Phys Lett* 2008; **92**: 261111.
33 Yang S, Astratov VN. Spectroscopy of coherently coupled whispering gallery modes in size-matched bispheres assembled on a substrate. *Opt Lett* 2009; **34**: 2057–2059.
34 Ashkin A, Dziedzic JM. Observation of resonances in the radiation pressure on dielectric spheres. *Phys Rev Lett* 1977; **38**: 1351–1354.
35 Kawata S, Tani T. Optically driven Mie particles in an evanescent field along a channeled waveguide. *Opt Lett* 1996; **21**: 1768–1770.
36 Fontes A, Neves AAR, Moreira WL, de Thomaz AA, Barbosa LC *et al*. Double optical tweezers for ultrasensitive force spectroscopy in microsphere Mie scattering. *Appl Phys Lett* 2005; **87**: 221109.
37 Ng J, Chan CT. Size-selective optical forces for microspheres using evanescent wave excitation of whispering gallery modes. *Appl Phys Lett* 2008; **92**: 251109.
38 Xiao JJ, Ng J, Lin ZF, Chan CT. Whispering gallery mode enhanced optical force with resonant tunneling excitation in the Kretschmann geometry. *Appl Phys Lett* 2009; **94**: 011102.
39 Svitelskiy O, Li Y, Darafsheh A, Sumetsky M, Carnegie D *et al*. Fiber coupling to $BaTiO_3$ glass microspheres in an aqueous environment. *Opt Lett* 2011; **36**: 2862–2864.
40 Oraevsky AN. Whispering-gallery waves. *Quantum Electronics* 2002; **32**: 377–400.
41 Colton D, Kress R. Integral equation method in scattering theory. New York: Wiley; 1983.
42 Yarovoy AG. Surface potential method in the wave scattering from localized inhomogeneities of a planar dielectric waveguide. *IEICE Trans Electron* 1995; **E78–C**: 1440–1446.
43 Boriskina SV, Nosich AI. Numerical simulation of surface-wave bandstop filters. *Microwave Opt Technol Lett* 1996; **13**: 169–173.
44 Hecht E. Optics. 4th ed. Reading, MA: Addison-Wesley; 2002. p56.
45 Brown J. Electromagnetic momentum associated with waveguide modes. *Proc IEEE* 1966; **113**: 27–34.
46 Laine JP, Little BE, Haus HA. Etch-eroded fiber coupler for whispering-gallery-mode excitation in high-Q silica microspheres. *IEEE Photon Technol Lett* 1999; **11**: 1429–1430.
47 Sumetsky M. Optimization of resonant optical sensors. *Opt Express* 2007; **15**: 17449–17457.
48 Lam CC, Leung PT, Young KJ. Explicit asymptotic formulas for the positions, widths, and strengths of resonances in Mie scattering. *J Opt Soc Am B* 1992; **9**: 1585–1592.
49 Fedorova KA, Cataluna M, Krestnikov I, Livshits D, Rafailov EU. Broadly tunable high-power InAs/GaAs quantum-dot external cavity diode lasers. *Opt Express* 2010; **18**: 19438–19443. Company contact: http://www.ccqed.eu/consortium/toptica/ (accessed 22 November 2012).
50 Li Y, Svitelskiy O, Carnegie D, Rafailov E, Astratov VN. Evanescent light coupling and optical propelling of microspheres in water immersed fiber couplers. *Proc SPIE* 2012; **8236**: 82361P. http://proceedings.spiedigitallibrary.org/proceeding.aspx?articleid=1344529.
51 Kanaev AV, Astratov VN, Cai W. Optical coupling at a distance between detuned spherical cavities. *Appl Phys Lett* 2006; **88**: 111111.
52 Fengnian X, Sekaric L, Vlasov YA. Ultracompact optical buffers on a silicon chip. *Nat Photon* 2007; **1**: 65–71.
53 Astratov VN, Ashili SP. Percolation of light through whispering gallery modes in 3D lattices of coupled microspheres. *Opt Express* 2007; **15**: 17351–17361.
54 Darafsheh A, Fardad A, Fried NM, Antoszyk AN, Ying HS *et al*. Contact focusing multimodal microprobes for ultraprecise laser tissue surgery. *Opt Express* 2011; **19**: 3440–3448.
55 Darafshesh A, Astratov VN. Periodically focused modes in chains of dielectric spheres. *Appl Phys Lett* 2012; **100**: 61123.
56 Schweiger G, Nett R, Weigel T. Microresonator array for high-resolution spectroscopy. *Opt Lett* 2007; **32**: 2644–2646.
57 Guzatov DV, Woggon, U. Coupled microsphere clusters for detecting molecule's dipole moment orientation. *Appl Phys Lett* 2009; **94**: 241104.
58 Francois A, Himmelhaus M. Optical biosensor based on whispering gallery mode excitations in clusters of microparticles. *Appl Phys Lett* 2008; **92**: 141107.

Supplementary Information for this article can be found on *Light: Science & Applications*' website (http://www.nature.com/lsa/)